JOURNAL OF GEOPHYSICAL RESEARCH, VOL. 113, D24210, doi:10.1029/2008JD010546, 2008

Radiative impact of mixing state of black carbon aerosol in Asian outflow

M. Shiraiwa,[1] Y. Kondo,[1] N. Moteki,[1] N. Takegawa,[1] L. K. Sahu,[1] A. Takami,[2] S. Hatakeyama,[3] S. Yonemura,[4] and D. R. Blake[5]

Received 4 June 2008; revised 29 September 2008; accepted 21 October 2008; published 25 December 2008.

[1] The radiative impact of the mixing state of black carbon (BC) aerosol is investigated in Asian outflow. The mixing state and size distribution of BC aerosol were measured with a ground-based single-particle soot photometer at a remote island (Fukue) in Japan in spring 2007. The mass concentration of BC in Asian continental air masses reached 0.5 μg m^{-3}, with a mass median diameter of 200–220 nm. The median value of the shell/core diameter ratio increased to ~1.6 in Asian continental and maritime air masses with a core diameter of 200 nm, while in free tropospheric and Japanese air masses it was 1.3–1.4. On the basis of theoretical calculations using the size distribution and mixing state of BC aerosol, scattering and absorption properties of PM_1 aerosols were calculated under both dry and ambient conditions, considering the hygroscopic growth of aerosols. It was estimated that internal mixing enhanced the BC absorption by a factor of 1.5–1.6 compared to external mixing. The calculated absorption coefficient was 2–3 times higher in Asian continental air masses than in clean air. Coatings reduced the single-scattering albedo (SSA) of PM_1 aerosol by 0.01–0.02, which indicates the importance of the mixing state of BC aerosol in evaluating its radiative influence. The SSA was sensitive to changes in air mass type, with a value of ~0.98 in Asian continental air masses and ~0.95 in Japanese and free tropospheric air masses under ambient conditions.

Citation: Shiraiwa, M., Y. Kondo, N. Moteki, N. Takegawa, L. K. Sahu, A. Takami, S. Hatakeyama, S. Yonemura, and D. R. Blake (2008), Radiative impact of mixing state of black carbon aerosol in Asian outflow, *J. Geophys. Res.*, *113*, D24210, doi:10.1029/2008JD010546.

1. Introduction

[2] Black carbon (BC) aerosol is a byproduct of incomplete combustion of fossil fuels and biomass. BC is a strong absorber of solar radiation; therefore, it is considered to make important contributions to the radiative forcing of the atmosphere. BC could be the second most important component of global warming after CO_2 in terms of direct forcing [*Jacobson*, 2000]. Furthermore, the semidirect effect of BC aerosol causes a heating of clouds, which results in the evaporation of cloud droplets and a reduction of the cloud albedo, thereby warming the surface [*Hansen et al.*, 1997; *Ackerman et al.*, 2000]. Absorption and scattering coefficients of aerosols are needed to model these effects.

[3] Freshly emitted soot is initially hydrophobic and mostly externally mixed with nonrefractory compounds; with time, it becomes hydrophilic and more internally mixed through condensation and coagulation. In polluted urban air, BC becomes internally mixed on a timescale of ~12 h with a coating of organics and sulfate [*Moteki et al.*, 2007; *Shiraiwa et al.*, 2007]. The radiative properties of BC depend strongly on the mixing state. *Schnaiter et al.* [2005] have investigated the absorption properties of BC coated with secondary organic aerosols. They found that the specific absorption cross section of internally mixed BC is amplified by a factor of about 2 compared to that of externally mixed BC. *Bond et al.* [2006] reported that the light-absorbing properties of BC could be enhanced by a factor of about 1.5 if BC is thickly coated with nonrefractory compounds, based on theoretical calculations. *Jacobson* [2000] conducted a model simulation and reported that the radiative forcing of BC is +0.27 W/m^2 when it is externally mixed, but this is enhanced to +0.54 W/m^2 when internally mixed. In addition, internally mixed BC aerosols act as cloud condensation nuclei (CCN) and are efficiently removed by wet deposition; hence, the coating of BC may change precipitation patterns and the spatial distributions of BC aerosols. Therefore, it is important to understand the mixing state of BC in order to evaluate its impact on climate. However, in situ measurements of the mixing state of BC of individual particles are still limited [*Schwarz et al.*, 2008].

[4] Because of the rapid economic development in East Asia, energy consumption is increasing, resulting in a higher rate of pollution emissions. It is reported that Asian aerosol sources are unlike those in Europe and North America: much

[1] Research Center for Advanced Science and Technology, University of Tokyo, Tokyo, Japan.
[2] National Institute for Environmental Studies, Tsukuba, Japan.
[3] Institute of Symbiotic Science and Technology, Tokyo University of Agriculture and Technology, Tokyo, Japan.
[4] National Institute for Agro-Environmental Sciences, Tsukuba, Japan.
[5] University of California, Irvine, California, USA.

0148-0227/08/2008JD010546$09.00

more coal and biomass are burned, leading to high emissions of BC and organic aerosol [*Huebert et al.*, 2003]. The emission estimates of BC were reported to be 1.05 Tg from China in the year 2000 [*Streets et al.*, 2003]. The major emission sources of black carbon are from the residential sector and biomass burning. An increase of emission leads to an increase of pollutants outflow from the Asian continent. Japan is located at the eastern edge of East Asia, and a westerly wind dominates in the winter-spring period [*Clarke et al.*, 2004; *Takami et al.*, 2005]. Therefore, transport of anthropogenic aerosols and trace gases to the western Pacific can affect the regional climate and air quality in this region, including Japan. It is of great interest therefore to study the physicochemical properties of BC aerosols in the Asian outflow. However, the size distribution and mixing state of BC aerosol in the Asian outflow remain poorly characterized.

[5] The objective of this study is to characterize the physicochemical properties of BC aerosol in the Asian outflow and evaluate the radiative impact of the mixing state of BC. The size distributions of BC and PM_1 aerosol were measured using a single-particle soot photometer (SP2). The mixing states of BC aerosol (coating thickness and coating materials) are quantified. On the basis of in situ measurements and Mie theory, absorption and scattering coefficients and the single-scattering albedo of PM_1 aerosol are computed. The dependence of the optical properties on mixing state of BC aerosol is investigated.

2. Configuration of the SP2

[6] A SP2 (Droplet Measurement Technologies, Boulder, Colorado) was used to measure the size and mixing state of single BC aerosol in real time using laser-induced incandescence (LII) technique. The basic measurement principle and schematic diagrams of the SP2 have been described previously [*Gao et al.*, 2007; *Moteki and Kondo*, 2007]. The SP2 consists of an intracavity Nd:YAG laser ($\lambda = 1.06\ \mu$m) and four optical detectors. The laser is in the TEM00 mode, with a Gaussian radial intensity distribution. Aerosol particles are dried prior to optical detection by dried sheath flow (RH < 4%) with a sheath/sample flow ratio of 10 and introduced to the laser beam vertically. BC aerosols passing through the laser beam elastically scatter laser light and at the same time absorb energy, are heated to their vaporization temperature, and incandesce. The incandescent light is detected by two photo multiplier tubes (PMTs) equipped with band-pass filters for different visible wavelength regions (λ = 350–500 nm and 400–750 nm). The blackbody temperature of a BC aerosol can be derived using the ratio of the LII signal intensity [*Moteki and Kondo*, 2007]. BC can be distinguished from incandescing non-BC aerosols such as metal particles on the basis of the boiling points of the particles [*Schwarz et al.*, 2006].

2.1. Determination of BC Diameter

[7] BC mass was measured using the BC mass and LII peak intensity relationship determined from calibration. The response of the LII detector was investigated using glassy carbon spheres (TOKAI Carbon Co., LTD, Tokyo, Japan and Alpha Aesar, Inc., Ward Hill, Massachusetts), graphite, and ambient BC aerosols in Tokyo. Dynamic shape factors (χ) of these particles were investigated using a differential mobility analyzer (DMA)-aerosol particle analyzer (APM) system [*McMurry et al.*, 2002]. The APM can measure the mass of particles using a combination of electrostatic and centrifugal forces [*Ehara et al.*, 1996]. A condensation particle counter (CPC) was used to monitor the number concentration. Ambient BC aerosols were heated to 400°C prior to introduction into the DMA-APM system to remove coating materials. BC density was assumed to be 1.77 g cm^{-3} [*Park et al.*, 2004]. Here χ is defined as the ratio of the actual resistance force of a nonspherical particle to the resistance force of sphere having the same volume (mass). For spherical particles, χ = 1, while for nonspherical particles $\chi > 1$. The χ values are summarized in Table 1. The χ values of glassy carbon particles are near 1, indicating they were nearly spherical in this size range. On the other hand, χ values of ambient BC aerosols were 1.7–2.2, indicating that they were aggregates.

Table 1. Shape Factors of BC Aerosols Used for LII Calibration

	GC(TOKAI)	GC(Alpha Aesar)	Graphite	Ambient BC
χ	1.0–1.2	1.0–1.1	1.3	1.7–2.2

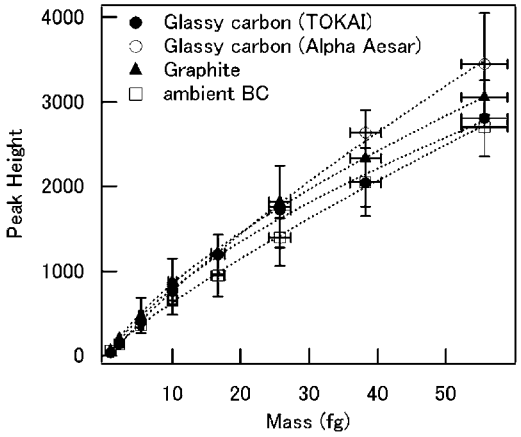

Figure 1. Calibration line of the LII detector using glassy carbon (TOKAI, Alfa Aesar), graphite, and ambient BC aerosols in Tokyo. Fitting lines are power functions (dotted line).

[8] For calibration, noncoated monodispersed BC aerosols that were size and mass selected by the DMA-APM system were introduced into the SP2. The mass transmission width of the DMA-APM system was narrower than ±6%. Multiply charged particles did not influence the calibration because those that had passed through the DMA were rejected by the APM. The relationship between the LII peak intensity and the mass of black carbon is shown in Figure 1, fitted by a power function. The scatter of the distribution of incandescence intensity for monodispersed BC aerosols caused an uncertainty in the peak height of ~21% (shown with error bars). The ±6% transmission width of DMA-APM system caused ~7% scatter in the distribution of peak height. The remaining uncertainty was attributed to the mean response of the SP2 to BC aerosols. The LII peak intensities depend on the type of black carbon over a ±20% range. The intensity of the LII signal is apparently dependent on emissivity (ε) and surface area of the particle [*Moteki and Kondo*, 2007]. If ε is linearly

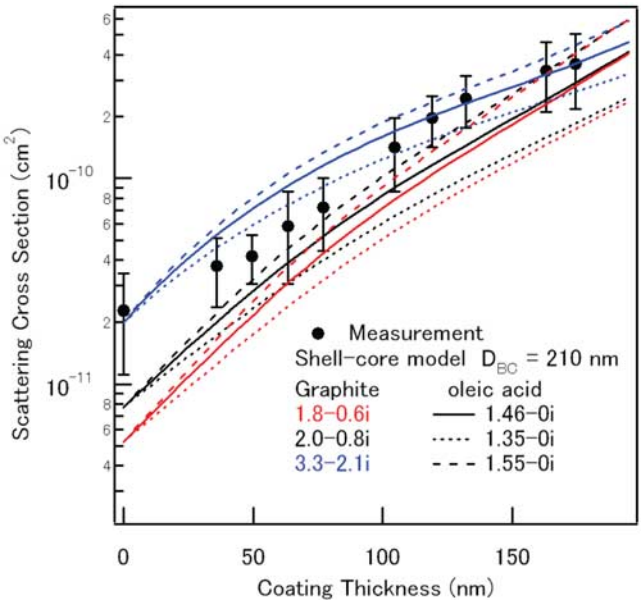

Figure 2. Scattering cross section of graphite (D_{BC} = 210 nm) coated by oleic acid obtained by coating experiments, along with theoretical calculations with various refractive indices of graphite and oleic acid. Bars indicate 25th to 75th percentile values.

proportional to diameter, the LII peak intensity measured by the SP2 becomes linearly proportional to the BC mass. However, our results show that the LII peak intensity depends not only on particle mass but also shows some variability depending on BC type, as discussed above. This can be due partly to the dependence of ε on particle morphology and composition. Considering the scatter of the LII intensity and dependence on black carbon type, the uncertainty of the LII peak intensity is 28%, resulting in an uncertainty of the derived BC mass of ~31%, which causes an uncertainty of the derived mass-equivalent core diameter (D_{BC}) of ~10%. For ambient measurements, the calibration data for ambient BC was used. The detection range of BC was 0.9–55 fg BC per particle, corresponding to a D_{BC} of 98–430 nm diameter with a density of 1.77 g cm^{-3}. The detection efficiency of BC aerosols by SP2 was 100% for particles larger than 150 nm in diameter and ~60% near the detection limit. For deriving the size distribution of BC aerosol, BC particles with diameters less than 150 nm were corrected considering the detection efficiency. BC aerosols larger than the upper limit were detected but not sized because of the saturation of the PMT detector.

2.2. Determination of Optical Size

[9] Scattered light was detected by two avalanche photodiodes (APD): the standard APD and a two-element avalanche photodiode detector (TEAPD) [*Gao et al.*, 2007]. For light-scattering aerosols, which do not incandesce (non-BC aerosol), the scattering signals were Gaussian. The peak intensity of the Gaussian scattering signal was proportional to the scattering cross sections of the particles, which were calibrated with measurements of polystyrene latex spheres (PSL) of known size. Conversion from scattering cross section to optical diameter was made using the Mie theory.

[10] For BC aerosols, the scattering signal was distorted because BC evaporates in the laser beam. The scattering properties of unperturbed BC aerosols were reconstructed by Gaussian fitting of the leading edge of the scattering signal (leading edge–only fit: LEO fit) [*Gao et al.*, 2007]. In this study, the last point of the leading edge was set to a triple Gaussian width away from the center position of the Gaussian. This fitting required the position information of the particles in the laser beam, which was enabled by TEAPD [*Gao et al.*, 2007]. Also required for the fitting was Gaussian width, which was predetermined by the scattering signal from the PSL. The relationship between the peak height of the full Gaussian scattering signal by the standard APD and the reproduced Gaussian peak height of that by the TEAPD show a tight linear correlation (r^2 = 0.99), indicating the validity of the LEO fit. The detection range of optical size was 200–750 nm.

[11] Coated BC particles with known core and shell diameters were introduced to the SP2 to quantify the optical size determination of coated BC. They were produced using the experimental system described by *Moteki and Kondo* [2007], which consists of a tandem differential mobility analyzer (TDMA) with a vapor condensing system. Glassy carbon (TOKAI) and graphite particles were used as cores, and glycerol and oleic acid were used as coating materials. Glycerol and oleic acid have different evaporative characteristics with the boiling points of 290°C and 360°C, respectively. Coated BC aerosols with D_{BC} of 150–400 nm and coating thicknesses of 25–400 nm were produced. The size transmission width of the DMAs was maintained to within ±6%. Doubly charged particles were also introduced to the SP2 but easily discriminated from singly charged particles because both core and shell diameters of doubly charged particles were about twice as large as those of singly charged particles.

[12] Figure 2 shows the experimental results of graphite particles coated by oleic acid with a D_{BC} of 210 nm, along with theoretical calculation of scattering cross sections using a shell-core model of Mie theory [*Bohren and Hoffman*, 1983]. The dielectric function was uncertain; therefore, various refractive indices of BC and oleic acid were assumed. The assumed values of the refractive indices of graphite and oleic acid were chosen on the basis of the work of *Moteki and Kondo* [2008]. The measured scattering cross sections agree well with those calculated within the uncertainty of the refractive indices. The measurements of other combinations of core (graphite and glassy carbon) and coating materials (glycerol and oleic acid) also agree well with the calculations, suggesting that the use of TEAPD and the shell/core model is reasonable to determine the scattering cross section of coated BC. The shell diameter of coated BC can be derived with ~15% error by conversion of the scattering cross section.

2.3. Determination of Mixing State of BC

[13] The mixing state, or the shell/core diameter ratio (R), was calculated by dividing the shell optical diameter by the core BC diameter. Considering the propagation of errors, the uncertainty of R was calculated to be ~18%. In deriving the distribution of R, the probability of reliable LEO fitting

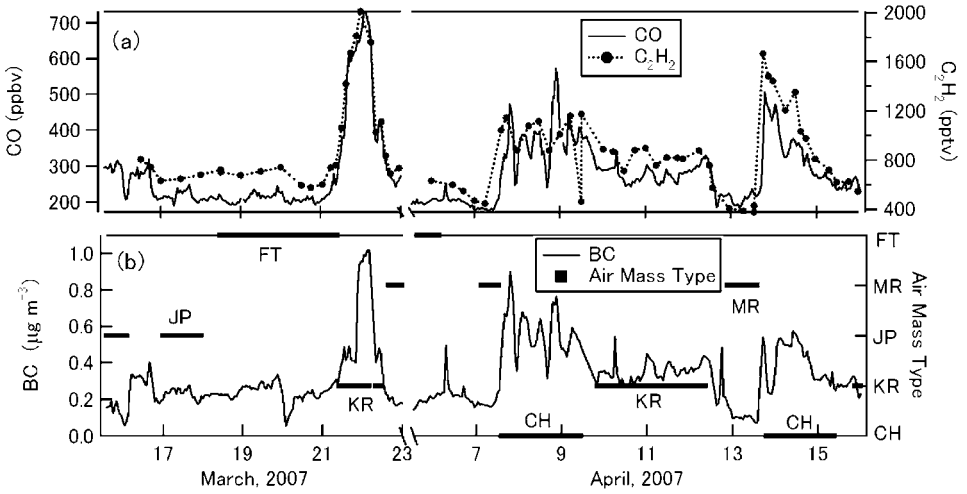

Figure 3. Time series plots of (a) C_2H_2 and CO and (b) BC with air mass type indicated.

was considered. The *R* values of some portions of BC could not be derived owing to unreliable LEO fitting near the detection limit (~200 nm) of the TEAPD. Fitting probabilities obtained by the coating experiment data were used in deriving the distribution of *R*.

3. Observation of Aerosols in Asian Outflow

3.1. Experimental Setup

[14] Ground-based measurements of aerosols and trace gases were performed at a remote site in Japan (Fukue Island, 32.8°N, 128.7°E) during 14–22 March and 5–16 April 2007. The site is located about 600 km east of the coastline of the Asian continent, about 250 km south of the Korean peninsula, and about 100 km west of Kyushu Island (Japan). The observatory house is located on the northwest side of Fukue Island. No significant local BC sources were identified [*Takami et al.*, 2005].

[15] The SP2 was deployed to measure BC and light-scattering aerosols. The sample air was aspirated from the roof of the observatory (3.8 m AGL) through a half-inch outer diameter stainless steel tube. Aerosols less than 2.5 μm were selected using a $PM_{2.5}$ cyclone. The sample air was introduced to the SP2 using quarter-inch copper tube with a sample flow rate of 50 mL min^{-1}. Size-resolved PM_1 aerosol chemical composition was analyzed using a quadruple aerosol mass spectrometer (Q-AMS; Aerodyne) [*Jayne et al.*, 2000]. Hydrocarbons were measured using a whole air sampling technique [*Simpson et al.*, 2003]. They were analyzed using gas chromatography (HP-6890) with flame ionization detection. The mixing ratio of carbon monoxide (CO) under ambient condition was measured using a nondispersive infrared absorption technique (Model48C, TECO, USA) [*Takegawa et al.*, 2006]. For the present analysis, all concentrations were merged into 1-h averages.

3.2. Classification of Air Masses

[16] Figure 3a shows time series plots of ethyne (C_2H_2) and carbon monoxide (CO). Ethyne is an excellent tracer for long-range pollution transport because it is a general product of incomplete combustion, with major sources from vehicles, biofuels, and biomass burning [*Streets et al.*, 2003]. The lifetime of ethyne is several weeks, which is sufficiently long to track plumes influenced by emissions from the Asian continent yet sufficiently short to provide strong pollution enhancements in these plumes relative to background [*Blake et al.*, 2003]. CO is also a good tracer of anthropogenic emissions, and CO and C_2H_2 showed similar variation. The concentrations of these species varied significantly, associated with changes in air masses origin, as discussed below in detail.

[17] Back trajectories were calculated to understand the observed variations associated with the different air mass origins. Calculations were made using the Meteorological Data Explorer (METEX; http://db.cger.nies.go.jp/metex/index.html) developed by the Center for Global Environmental Research (CGER) using data from the National Centers for Environmental Prediction (NCEP). Back trajectories using 3D wind fields initialized by H = 500 m were calculated with a total run time of 96 h (4 days) for every hour during the campaign periods. Observed air masses were distinctly classified into 5 types by region of origin and transport pathway: China (19%), Korea (17%), Japan (11%), Marine (10%), and Free Troposphere (FT) (20%). The fraction of each observed air mass type is also shown in parentheses, summing up to 77%. Note that the remaining 23% of air masses were classified as transition periods and excluded in the analysis. On 16 March and 6 April, new particle formation events were observed, and these periods were also classified as transition periods. Back trajectories of each air mass are shown in Figure 4. The ambient temperature, relative humidity, and CO concentration have also been analyzed and are summarized in Table 2. Classifications of air masses were mainly based on back trajectories but also supported by trace gases and meteorological parameters, as discussed below.

3.2.1. China (CH)

[18] CH air masses originated in the northern region of China (35°N–45°N, 110°E–120°E) and passed over Beijing and Tianjin, which are large emission sources in China. Trajectories passed over the Yellow Sea and then through the southwest edge of the Korean peninsula, which has only small emission source according to the emission

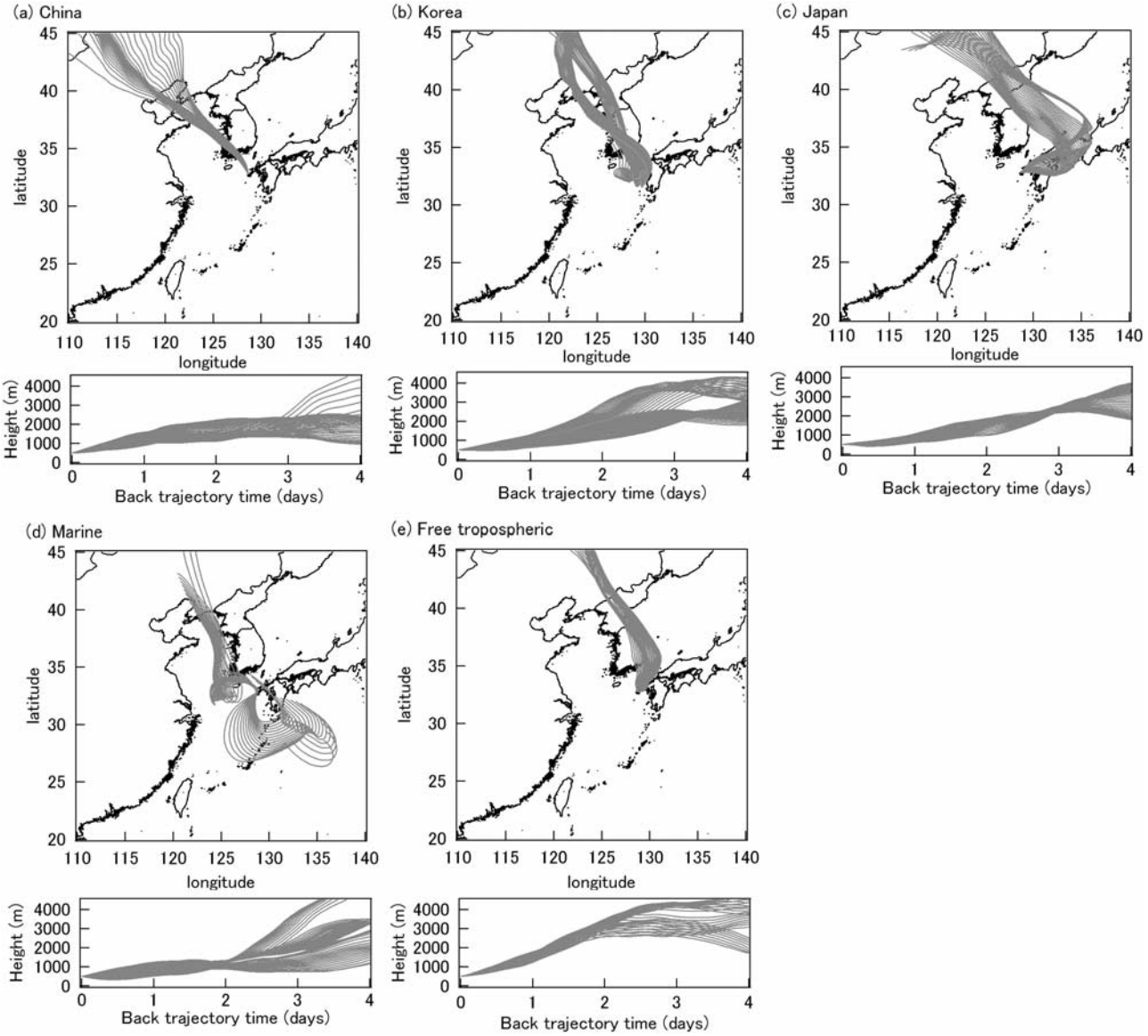

Figure 4. Horizontal and vertical plots of back trajectories of air masses of the following types: (a) China, (b) Korea, (c) Japan, (d) marine, and (e) free troposphere.

inventory [*Streets et al.*, 2003; *Sahu et al.*, 2008]. A high-pressure system was located near the Chinese coast during this period. The high CO concentration air masses were transported by winds that flowed along the edge of the high-pressure system. The highest CO mixing ratio (356 ppbv) suggests the large influence of anthropogenic emissions in China.

3.2.2. Korea (KR)

[19] KR air masses originated from northeastern region (40°N–45°N, 120°E–130°E) of China and passed through

Table 2. Statistics of Aerosols and Trace Gases in Five Different Air Mass Types[a]

Species	China	Korea	Japan	Marine	Free Troposphere
Temperature (°C)	13.4 (13.9 ± 1.7)	13.3 (13.5 ± 1.5)	9.9 (9.8 ± 1.0)	14.1 (14.7 ± 3.6)	9.9 (9.9 ± 1.3)
RH (%)	59 (61 ± 11)	53 (57 ± 12)	63 (60 ± 13)	69 (68 ± 9)	52 (54 ± 8)
CO (ppbv)	356 (359 ± 72)	285 (294 ± 48)	267 (255 ± 39)	217 (225 ± 37)	208 (210 ± 14)
BC (μg m^{-3})	0.51 (0.50 ± 0.14)	0.36 (0.42 ± 0.18)	0.23 (0.23 ± 0.08)	0.17 (0.16 ± 0.05)	0.23 (0.24 ± 0.05)
SO_4^{2-} (μg m^{-3})	10.0 (11.3 ± 5.8)	6.7 (7.6 ± 2.8)	6.3 (5.7 ± 3.2)	7.6 (7.8 ± 3.4)	3.5 (3.3 ± 1.0)
Organics (μg m^{-3})	8.6 (8.6 ± 2.3)	5.9 (5.7 ± 1.0)	3.4 (2.9 ± 1.1)	2.5 (2.5 ± 0.6)	3.5 (3.5 ± 0.9)
NO_3^- (μg m^{-3})	0.83 (0.95 ± 0.49)	0.58 (0.60 ± 0.21)	0.28 (0.33 ± 0.18)	0.21 (0.23 ± 0.11)	0.32 (0.46 ± 0.33)
NH_4^+ (μg m^{-3})	3.4 (3.7 ± 1.6)	2.6 (2.8 ± 0.9)	1.6 (1.5 ± 0.8)	2.0 (2.1 ± 0.8)	1.3 (1.2 ± 0.4)

[a]Statistics given in format median (mean ± standard deviation).

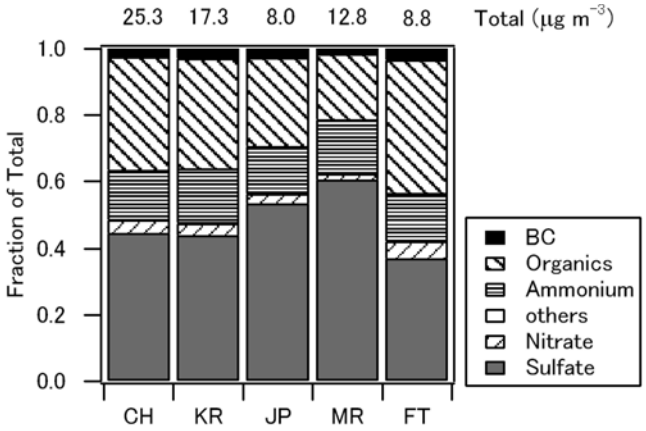

Figure 5. Average chemical composition of PM_1 aerosols measured in the different air masses.

the Korean peninsula. These air masses were mainly affected by Korean emissions, because the emission of BC in the northeastern region of China was small on the basis of emission inventory and the majority of air masses passed through Seoul or Pusan, which have large emission sources on the Korean peninsula. During the KR period, a high-pressure system was located over the Yellow Sea.

3.2.3. Japan (JP)

[20] JP air masses originated from the northeastern region of China and passed over North Korea. Trajectories tracked down the Japanese mainland, and then went west to reach the sampling site. Because the anthropogenic emissions of the northeastern region of China and North Korea are small, these air masses were influenced primarily by fresh Japanese emissions. During JP periods, the Siberian High was centered near 50°N, 110°E.

3.2.4. Marine (MR)

[21] MR air masses originated from the East Japan Sea in March and from the Yellow Sea in April. They spent at least 2 days over the sea prior to sampling. We note that this MR air mass type was different from typical clean marine air masses, as they were influenced by Asian emissions. The MR air masses were associated with low-pressure or frontal systems passing over Fukue Island, which brought relatively clean air over the ocean for example on 13 April as shown in Figure 3. The highest ambient temperature (14.7 (±3.6) °C) and relative humidity (68 (±9) %) confirm the identity of marine air.

3.2.5. Free Troposphere (FT)

[22] FT air masses were transported from the free troposphere (at an altitude greater than 2–3 km) over the continent by northerly winds; these air masses then descended to the boundary layer over the eastern edge of the Korean peninsula. The lowest values of ambient temperature (9.9 (±1.3) °C) and relative humidity (54 (±8) %) confirm the free tropospheric origin of the air masses.

[23] The concentration of CO was higher in CH and KR air masses as shown in Table 2, as compared with JP, MR, and FT air masses. These high CO concentrations are likely due to transport from areas with high emission rates in China and Korea.

3.3. Distribution of BC and Other Aerosols

[24] Time series plots of mass concentration of BC along with air mass types are shown in Figure 3b. The BC mass concentration in PM_1 was derived from BC mass size distributions approximated by a lognormal function, as explained in section 4.1. The average (±standard variation) concentration in the campaign period was 0.32 (±0.17) μg m^{-3}. A large range of variation of 0.1–1.0 μg m^{-3} was observed owing to variations in air masses with different characteristic BC concentrations. The BC concentration showed large enhancements of ~1.0 μg m^{-3} on 22 March and 8–9 April, which corresponded to Korean and Chinese air masses, respectively.

[25] Distributions of BC and inorganic and organic aerosols are summarized in Table 2. CH air masses had the highest concentration of BC, with a mass concentration of 0.50 (±0.14) μg m^{-3}, followed by KR air masses: MR air masses had the lowest value of 0.16 (±0.05) μg m^{-3}. Concentrations of aerosols essentially showed the highest values in CH and KR air masses, because both are strongly influenced by anthropogenic emissions and showed lower values in JP, MR, and FT air masses. The average chemical compositions are shown in Figure 5. Sulfate and organics are the main constituents, while BC aerosol accounted for 1–4% in the mass of PM_1 aerosols in every air mass type.

4. Physicochemical Properties of Aerosol

4.1. Size Distribution

[26] Figure 6 shows the average BC mass (Figure 6a) and number size (Figure 6b) distributions for the air mass types measured using the SP2. To estimate the whole size distribution, a single, lognormal distribution was assumed, which has been observed in Asian outflow in the free troposphere by *Clarke et al.* [2004]. Mass median diameters (MMD) were 200–220 nm and number median diameters were 120–140 nm in every air mass type. These MMDs were in a size range similar to those obtained by SP2 measurements in the free troposphere [*Schwarz et al.*, 2006, 2008] and the lower troposphere [*Moteki et al.*, 2007]. The mass concentration of BC aerosol was calculated by integrating the fitted lognormal functions.

[27] Average volume size distributions of light-scattering aerosol in the air masses measured using the SP2 are shown in Figure 7. Light-scattering aerosols are non-BC aerosols whose components are sulfate, organics, nitrate, and ammonium, based on the AMS measurements. The mass of light-scattering aerosol was derived by integrating the fitted lognormal function assuming a density of 1.8 g/cm^3. A single lognormal distribution was also assumed as was done for BC. The correlation between measured AMS mass concentrations versus estimated SP2 light-scattering aerosol mass showed a good linear correlation (r^2 = 0.84) with a slope of 0.7. The 30% difference can be partly due to the difference of definition of diameter (AMS: aerodynamic diameter; SP2: optical diameter) and the uncertainty of the assumed particle density. The MMDs were ~500 nm in CH and KR air masses, which were larger than that of ~350 nm in MR, JP, and FT air masses. This is likely due to condensation and coagulation during transport in the CH and KR air masses. The concentration was lowest in the FT

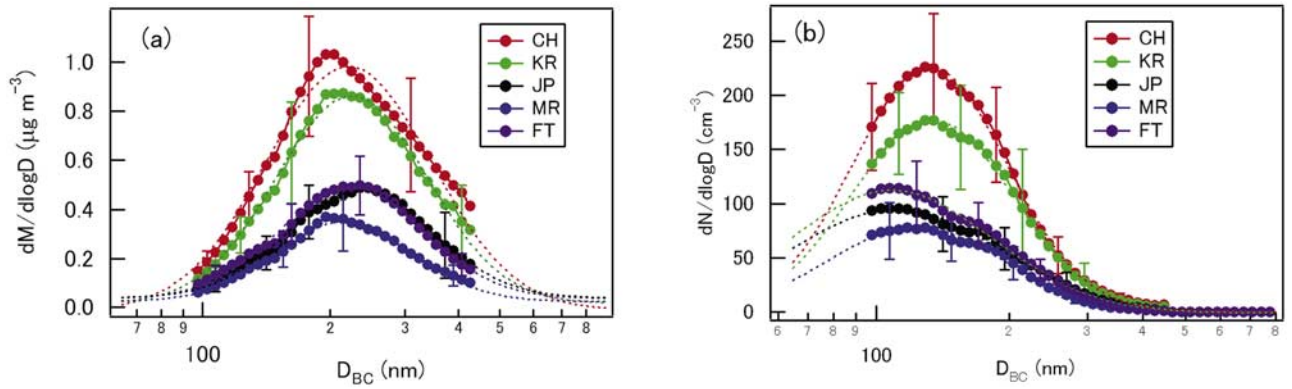

Figure 6. Average (a) mass and (b) number size distributions of BC observed by the SP2 in air masses of China (CH), Korea (KR), Japan (JP), marine (MR), and the free troposphere (FT). Lognormal functions were fitted to the data for sizes of 98 nm < D_{BC} < 430 nm. Bars show the 1σ values.

air masses, which was likely due to deposition and dilution process during transport in the free troposphere.

4.2. Mixing State of BC Aerosol

4.2.1. Shell/Core Diameter Ratio

[28] Time series plots of normalized distributions of the shell/core diameter ratio (R) with D_{BC} = 200 (±10) nm are shown in Figure 8. The median value is also plotted, showing the changes with different air masses. The median value of R with D_{BC} = 300 (±10) nm showed similar temporal variations to that for D_{BC} = 200 (±10) nm; however, the average value was smaller. The smaller R is due to the larger amount of coating materials required to increase R by the same degree at larger D_{BC}. Median values of R with D_{BC} = 200 and 300 nm are summarized in Table 3.

[29] Average distributions of R with D_{BC} = 200 (±10) nm in each air mass type are shown in Figure 9. In CH and KR air masses, the median R with a diameter of 200 nm was ~1.6, which indicates the most BC aerosols were thickly coated. This could have resulted from condensation of organic and inorganic components during the transport from China and Korea. It is also possible that BC was coated to some extent already in China and Korea, depending on the time during which air masses remains after BC emissions. On the basis of back trajectory analysis, the transport time from the Asian continent to the sampling site was long enough (2–3 days) for the condensation on BC to proceed. The mass concentrations of organic and inorganic aerosols were much higher in CH and KR air masses (Table 2), which should result in thicker coatings on BC aerosols. In MR air masses, BC was also thickly coated with a median R of ~1.6. The surface of BC aerosol could be hydrophilic under humid conditions (RH = 70%) [*Mikhailov et al.*, 2006] in MR air masses and thus coatings could condense on BC aerosol easily.

[30] In contrast, in JP and FT air masses, the median values were 1.3–1.4, which indicates that large amounts of BC aerosols in these air masses were noncoated or thinly coated compared to other air mass types. The transport time from the Japanese main island to the sampling site was about 6 h based on back trajectory analysis. It is reported that BC is coated on a timescale of about 12 h in urban polluted air [*Moteki et al.*, 2007; *Shiraiwa et al.*, 2007]. Therefore, the transport time of about 6 h is too short for full aging in JP air masses. Moreover, the mass loadings of organics and inorganic aerosol components, which possibly contributed to coatings, were smaller in JP and FT air masses than those in CH and KR air masses (Table 2).

4.2.2. Coating Materials on BC

[31] To investigate the contribution to the coating on BC aerosols by sulfate, organics, and nitrate measured by AMS, Positive Matrix Factorization (PMF) [*Paatero and Tapper*, 1993] was applied. The same method has been used in previous studies [*Shiraiwa et al.*, 2007]. The ratio of the mass concentrations of sulfate, organics, and nitrate to those of BC (X/BC, X = sulfate, organics, and nitrate) and the median value of R with D_{BC} = 200 (±10) nm were applied to the PMF analysis. We assumed that the coating composition matches the bulk aerosol composition. We used X/BC instead of absolute mass loadings, because it represents the relative amount of coating materials to BC aerosols [*Moteki et al.*, 2007]. The parameters (sulfate/BC, organics/BC, nitrate/BC, and the median value of R) predicted by the PMF model agree quite well with those observed, with r^2

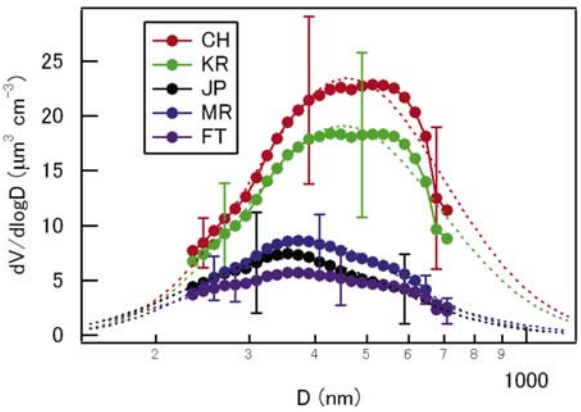

Figure 7. Average volume size distribution of scattering aerosol in the air masses. Lognormal functions were fitted to the data for sizes of 230 nm < D_{BC} < 700 nm. Bars show the 1σ values.

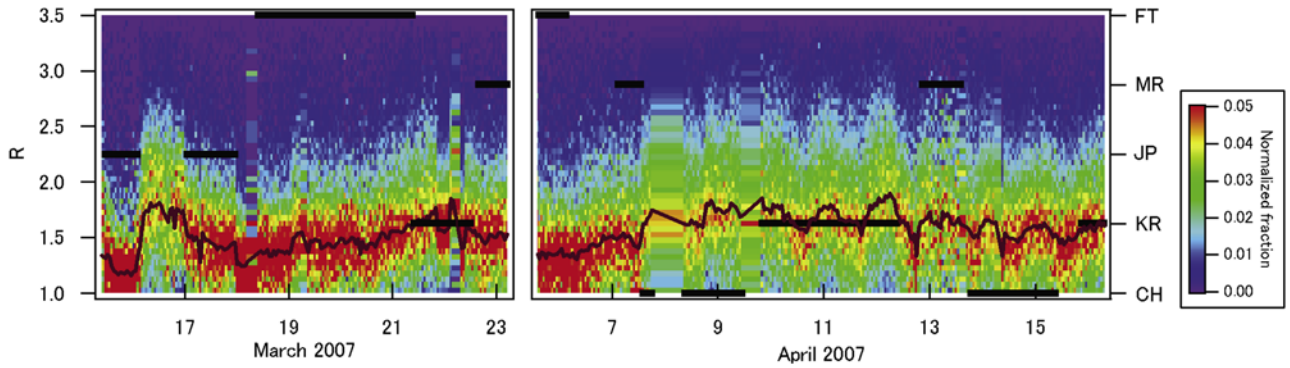

Figure 8. Time series image plots of the distribution of R with D_{BC} = 200 (±10) nm along with air mass type (indicated by horizontal lines corresponding to the air mass types indicated on the right ordinate). The brown lines indicate the median values of R.

values for the correlations between the observed and predicted values of 0.97, 0.61, 0.95, and 0.98, respectively.

[32] The three-factor PMF model resulted in physically interpretable factors (Figure 10a). On the y axis is the explained variation, which is a quantitative, dimensionless number of how important each factor is in explaining each parameter [*Paterson et al.*, 1999]. Factor 1, which explains 94% of sulfate/BC and 19% of R, indicates that sulfate was the principal contributor to the coatings in this factor. Factor 2 explains 31% of organics/BC and 68% of R, which means that organics were the main contributor in this factor. On the other hand, nitrate was considered to be the main contributor to coatings in factor 3. We note that factors 1 and 3 also contain some contributions from organics/BC ratio. Therefore, organics are considered to be a subcontributor to factors 1 and 3. The cumulative variance shows that the use of the three factors explains almost the entire variance (>95%) in every parameter.

[33] Figure 10b shows the time series of normalized factor contributions to the median value of R (D_{BC} = 200 nm) along with air mass type. Factors 1 and 2 were the dominant contributors over the entire period, indicating that organics and sulfate contributed to the coatings dominantly. These two factors accounted for 87% of the coating on BC aerosols according to the cumulative variance of R (Figure 10a). At nighttime, the contribution of factor 3 showed an enhancement of as high as 30%, for example on 15 March, 19 March, and 14 April. In these periods, the relative humidity was around 80%. The equilibrium of the nitric acid (HNO_3) reaction with ammonia (NH_3) to form ammonium (NH_4^+) and nitrate (NO_3^-) shifts toward the aerosol phase at high ambient RH [*Morino et al.*, 2006]. This explains the larger contribution of nitrate to the coating under high relative humidity conditions, as also observed in the outflow from Tokyo [*Shiraiwa et al.*, 2007]. On 14 April, the contribution of factor 1 showed an enhancement as high as 70% in the MR air mass (Figure 10b), which indicated the large contribution of sulfate to coatings. The variability of factor contributions reflects the different sources/mechanisms that can be associated with the different meteorological conditions and air mass types.

Table 3. Median (±Standard Deviation) Values of R With D_{BC} = 200 and 300 nm

	200 nm	300 nm
CH	1.6 ± 0.1	1.4 ± 0.1
KR	1.6 ± 0.1	1.4 ± 0.1
JP	1.3 ± 0.1	1.2 ± 0.2
MR	1.6 ± 0.1	1.4 ± 0.1
FT	1.4 ± 0.1	1.2 ± 0.1

5. Radiative Influence

[34] The absorption coefficient (k_{abs}), scattering coefficient (k_{sca}), and single-scattering albedo (SSA) of PM_1 aerosol at a wavelength of 550 nm under both dry and ambient RH condition were calculated to investigate the radiative impacts of BC aerosol in the Asian outflow. One hour–averaged k_{abs} and k_{sca} were calculated by $k = \int \sigma(D, R) \cdot \frac{dN}{d \log D}\, dR \cdot d \log D$, where $\sigma(D, R)$ is the absorption or scattering cross section and $dN/d\log D$ is the 1-h-averaged aerosol number size distribution. In calculating $\sigma(D, R)$, we have applied the shell/core model of Mie theory, which was reported to be a good proxy for internally mixed BC with arbitrary eccentricity, compared to effective medium theories [*Schnaiter et al.*, 2005]. SSA was calculated as SSA = $k_{sca}/(k_{sca} + k_{abs})$. To investigate the sensitivity of mixing state of BC aerosol to these radiative parameters, two cases

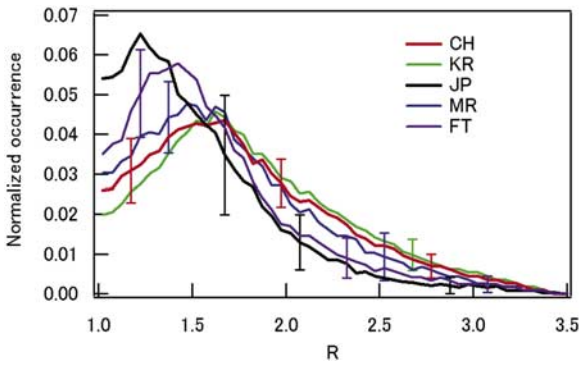

Figure 9. Average normalized distributions of R with D_{BC} = 200 (±10) nm in the five air mass types.

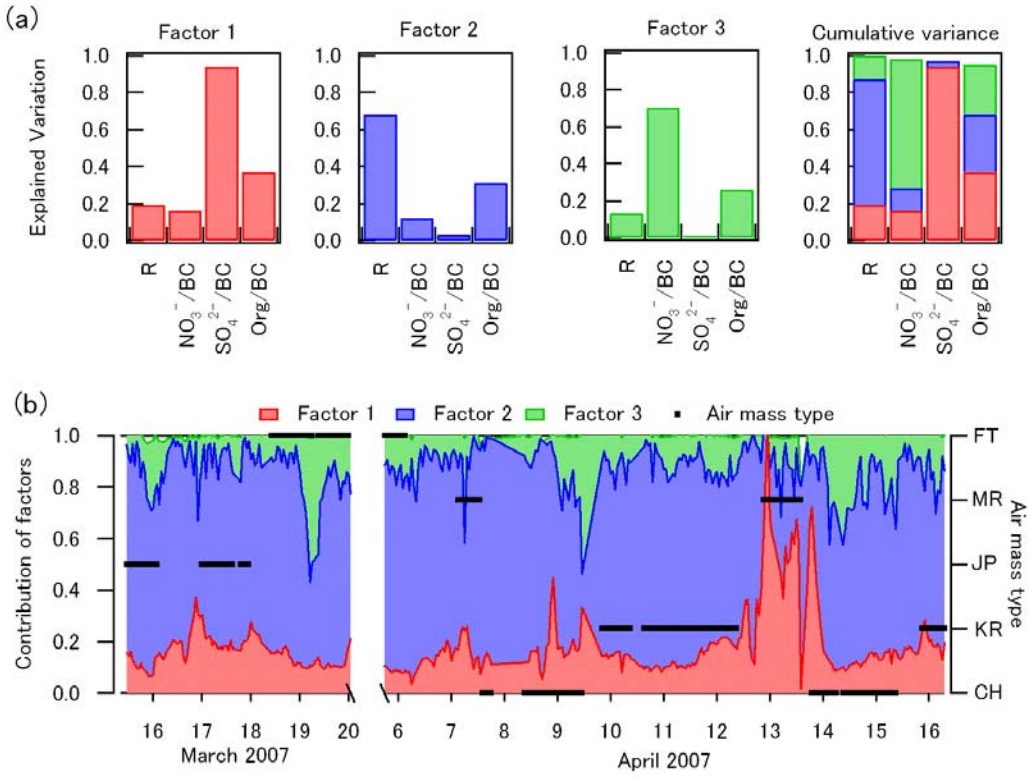

Figure 10. Explained variation of the median values of R (D_{BC} = 200 nm), nitrate/BC, sulfate/BC, and organics/BC in the three-factor PMF model. In addition to factors 1, 2, and 3, the cumulative variance explained by the PMF analysis is also shown. (b) Time series of normalized factor contributions for the median value of R (D_{BC} = 200 nm) along with air mass type.

that assumed the external and internal mixing of BC aerosol were considered. In the internal mixing case, the mixing state of BC aerosol was considered using the observed shell/core diameter ratio, whereas BC aerosol was assumed to be entirely noncoated in the external mixing case.

[35] To compute the radiative parameters under ambient condition, water uptake on coated BC and light-scattering aerosol was estimated using the thermodynamic equilibrium model for multiphase, multicomponent inorganic aerosols, ISORROPIA [*Nenes et al.*, 1998]. Aerosol-phase concentrations of SO_4^{2-}, NO_3^-, and NH_4^+, and temperature and RH were used as input parameters for the model calculations. The water uptake increased the diameter of light-scattering aerosols by 25 (±8)% and increased the coating thickness of coated BC aerosol by 30 (±9)%, mainly depending on the RH. Organics, which were also a main component of light-scattering aerosol and coatings, were not included in this model. Organics are known to exhibit some hygroscopicity; however, it has been reported that the hygroscopic growth factor of organics is much smaller than inorganic components and the contribution of the organics to the overall water uptake is mostly of minor importance [*Kleindienst et al.*, 1999]. *Gysel et al.* [2007] estimated that inorganic components contribute to the hygroscopic water uptake by more than 80% and the organic contribution to water uptake is minor (<20%) in aged-polluted and clean-background air masses. We assumed that the presence of organics in the aerosol did not significantly affect the hygroscopic properties of the aerosol.

5.1. Absorption Coefficient

[36] The fitted lognormal distribution in Figure 6 was used as the size distribution of BC aerosol. The refractive indices (m) of BC aerosol in three cases were used to investigate the sensitivity to k_{abs}: m = (2, 1) [*Janzen*, 1979], (1.87, 0.56), and (1.47, 0.34) [*Marley et al.*, 2001]. Other published values are within the range of these values [*Bond and Bergstrom*, 2006]. The calculated k_{abs} showed variability of ~20%, depending mainly on the imaginary part of m. In further analysis, we used the middle value of (1.87, 0.56), in which the uncertainty of r cause ~20% error in deriving k_{abs}. For dry conditions, the coatings were assumed to be organics and sulfate on the basis of the discussion in section 4.2.2. For ambient conditions, water is also a coating component, increasing the coating thickness by ~30%. The m of water, organics, and ammonium sulfate at a wavelength of 0.5 μm have been reported to be m = (1.34, 0), (1.45, 0), and (1.52, 0) [*Krekov*, 1993], respectively. We assumed an average m value of coatings under dry conditions of m = (1.5, 0). To investigate the uncertainty associated with this assumption, m = (1.45, 0) was also tested, resulting in a calculated k_{abs} of ~3% lower value. Therefore, the m of coatings was not a critical parameter in deriving k_{abs}, which caused only about 3% uncertainties.

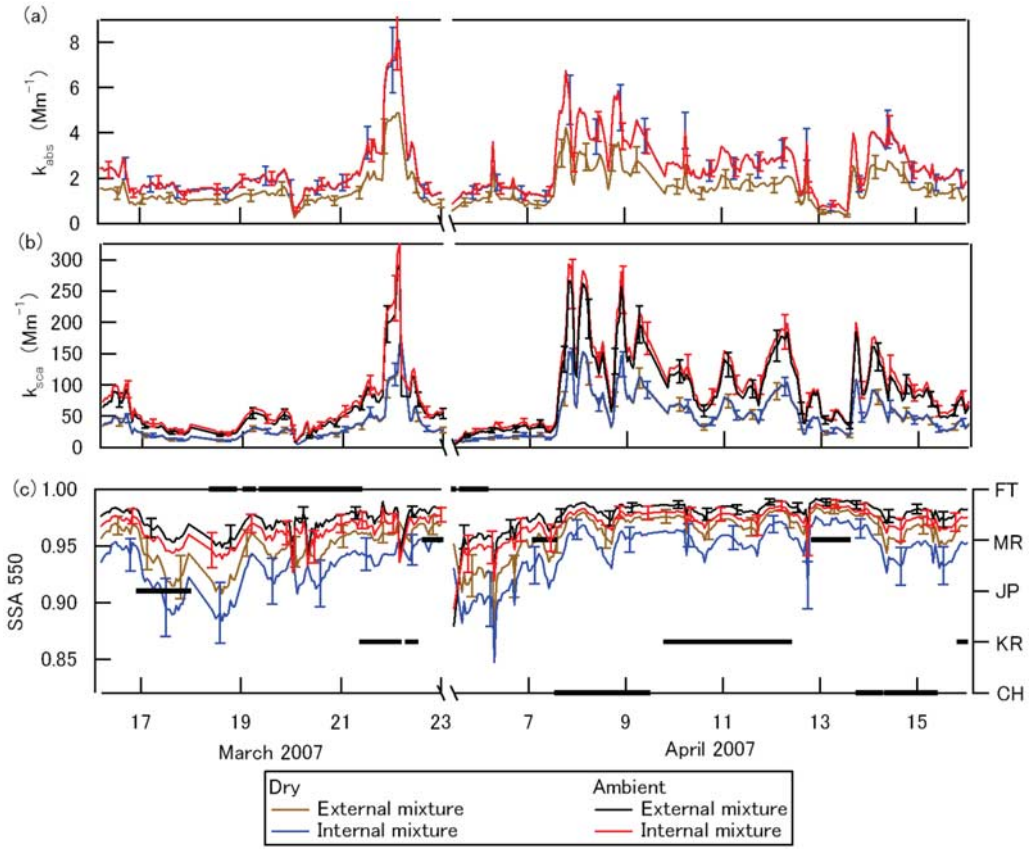

Figure 11. Time series plots of (a) k_{abs}, (b) k_{sca}, and (c) SSA of PM_1 aerosol (λ = 550 nm). External and internal mixture cases are shown under dry and ambient conditions.

The m under ambient condition was assumed to be m = (1.45, 0) considering the reduction of m by water uptake.

[37] The mixing state was directly measured in the D_{BC} range of 150–400 nm, as discussed in sections 2 and 4.2.1. In calculating the optical properties, we have used 1-h-averaged distribution of the shell/core diameter ratio as shown in Figure 8. They were derived for values of D_{BC} of 150(±25), 200(±25), 250(±25), 300(±25), and 350(±25) nm. The mixing state for D_{BC} < 150 nm (D_{BC} > 400 nm) was assumed to be the same as for D_{BC} = 150 nm (D_{BC} = 350 nm). To assess the uncertainties associated with this assumption, a case in which BC was assumed to be noncoated outside the D_{BC} = 150- to 400-nm range was calculated, resulting in an about 8% lower value. This case was the lower limit of absorption enhancement by coatings. Therefore, the assumption of mixing state beyond the detection ranges was estimated to cause about 8% uncertainty.

[38] The time series of calculated k_{abs} are shown in Figure11a. k_{abs} showed a variability similar to the mass concentration of BC aerosol shown in Figure 3b. The distributions of k_{abs} with air mass type are shown in Figure 12a and summarized in Table 4. The calculated k_{abs} in internal mixtures was 1.6 times higher than that in external mixtures in CH, KR, and MR air masses and 1.5 times higher than that in JP and FT air masses. This clearly shows the importance of considering BC mixing state for the evaluation of absorption properties.

[39] The calculated k_{abs} for internal mixing under dry and ambient conditions were almost the same value. One reason is the reduction of the refractive index of coating by water coatings from 1.5 to 1.45, which leads to a ~4% reduction of absorption cross section. Another reason is the saturation of the absorption enhancement by coatings [*Bond et al.*, 2006]. The absorption increases as coatings condense on the BC core, however, when coatings become thicker, the absorption enhancement reaches a maximum amplification. Because the coatings were relatively thick (R~1.4–1.6) under dry conditions and water reduced the refractive index, the water uptake did not increase the absorption enhancement significantly. The k_{abs} values were 2–3 times higher in CH and KR air masses compared to those in JP, MR, and FT air masses mainly because of higher BC concentrations.

5.2. Scattering Coefficient

[40] The k_{sca} of PM_1 aerosol was calculated by summing that of light-scattering and BC aerosols. Most light-scattering aerosols were composed of sulfate and organics, on the basis of the AMS measurements, and the m of light-scattering aerosols under dry and ambient conditions was assumed to be (1.5, 0) and (1.45, 0), respectively. The sensitivities of k_{sca} to m were investigated by assuming m

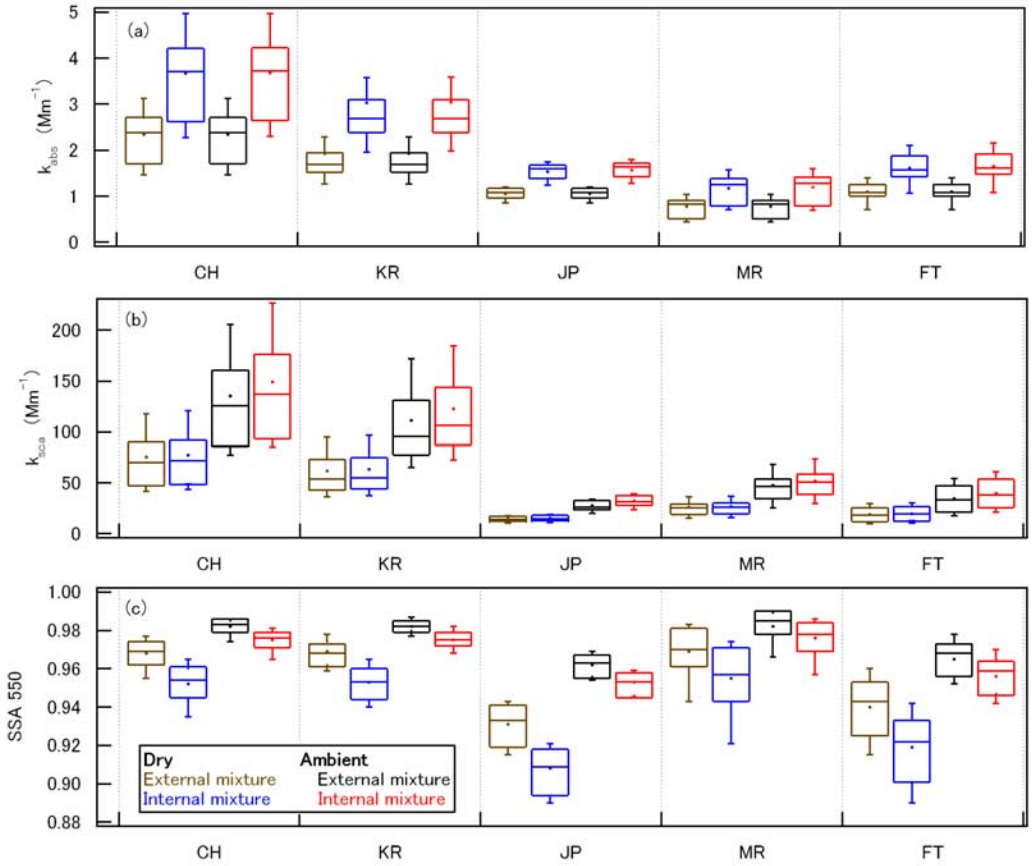

Figure 12. Distribution of (a) k_{abs}, (b) k_{sca}, and (c) SSA of PM_1 aerosol (λ = 550 nm) in different air masses.

of (1.55, 0) and (1.45, 0) under dry conditions, resulting in a variability of ~15%. The k_{sca} of BC aerosol was also calculated assuming external and internal mixture cases. k_{sca} of PM_1 aerosol was dominated by the k_{sca} of light-scattering aerosols and k_{sca} of BC contributed to PM_1 k_{sca} by only ~3% and ~6% in external and internal cases, respectively.

[41] Time series of calculated k_{sca} are shown in Figure 11b and the statistical value of k_{sca} in each air mass is shown in Figure 12b and Table 4. k_{sca} of the internal mixture showed a slightly larger value (~3%) than that in external mixture. Because of water uptake, k_{sca} under ambient conditions was estimated to be about twice as large as that under dry conditions. The calculated k_{sca} showed the highest value of 150 Mm^{-1} in CH air masses. *Clarke et al.* [2004] reported a k_{sca} in Asian outflow of ~140 Mm^{-1} in the lower atmosphere in spring 2001, which is comparable to this study. Calculated k_{sca} showed lower values of ~30 Mm^{-1} in JP and FT air masses, which was attributed to a lower concentration of light-scattering aerosol in these air masses, as shown in Figure 7.

5.3. Single-Scattering Albedo

[42] Figure 11c shows the time series plots of the calculated SSA under dry and ambient conditions for external and internal mixture cases. The error bars represent the propagation errors of k_{sca} (~15%) and k_{abs} (~20%). Under ambient conditions in the internal mixture case, SSA ranged from 0.91 to 0.99. *Nakajima et al.* [2007] reported that the SSA at λ = 500 nm at Fukue was in the range of 0.90 to 0.98 in spring 2005, which is comparable to this study. The statistical value of SSA is shown in Figure 12c and in Table 4. Owing to the absorption enhancement by coatings, the SSA values were reduced by 0.01–0.02 with internal mixing compared to that with external mixing under both dry and ambient conditions. This corresponds to an increase of coalbedo by 0.01–0.02. SSA values were lower in JP and FT air masses compared to those in CH, KR and MR air masses, because of the low value of k_{sca}, even though k_{abs} was not high.

[43] It has been reported that the critical SSA at which the aerosol impact on surface temperature shifts from cooling to heating is 0.90–0.93 based on modeling studies [*Hansen et al.*, 1997; *Cook and Highwood*, 2004]. In the case of external mixing, SSA was larger than the critical SSA, whereas with internal mixing SSA was comparable to the critical SSA in the JP and FT air masses during 18–21 March and 5 April. The low value of SSA in FT air masses implies that SSA was also low in the free troposphere. Thus, absorption of solar visible radiation by BC aerosol in the Asian outflow would reduce the local low cloud amount and result in positive climate feedback. However, near-surface properties of SSA do not always provide a good representation of the atmospheric column [*Clarke et al.*, 2004].

Table 4. Absorption Coefficient, Scattering Coefficient, and Single Scattering Albedo in Each Air Mass Type Under Dry and Ambient Conditions With Internal and External Mixing[a]

	k_{abs} (Mm^{-1})				k_{sca} (Mm^{-1})				SSA			
	Dry		Ambient		Dry		Ambient		Dry		Ambient	
	Internal	External	Internal	External	Internal	External	Internal	External	Internal	External	Internal	External
CH	3.67 ± 1.08	2.35 ± 0.66	3.68 ± 1.06	2.35 ± 0.66	77.5 ± 31.2	75.6 ± 30.7	149 ± 58	135 ± 54	0.95 ± 0.01	0.97 ± 0.01	0.97 ± 0.01	0.98 ± 0.01
KR	3.03 ± 1.30	1.93 ± 0.83	3.04 ± 1.30	1.93 ± 0.83	63.4 ± 25.6	61.8 ± 25.0	123 ± 49	111 ± 45	0.95 ± 0.01	0.97 ± 0.01	0.97 ± 0.01	0.98 ± 0.01
JP	1.53 ± 0.23	1.05 ± 0.30	1.57 ± 0.23	1.05 ± 0.30	15.4 ± 3.0	14.7 ± 3.0	32.3 ± 6.1	27.8 ± 5.5	0.91 ± 0.01	0.93 ± 0.01	0.95 ± 0.01	0.96 ± 0.01
MR	1.18 ± 0.35	0.79 ± 0.24	1.20 ± 0.36	0.79 ± 0.24	26.7 ± 7.8	26.1 ± 7.7	51.9 ± 15.3	47.7 ± 21.5	0.96 ± 0.02	0.97 ± 0.01	0.98 ± 0.01	0.98 ± 0.01
FT	1.61 ± 0.37	1.10 ± 0.25	1.65 ± 0.38	1.10 ± 0.25	19.8 ± 8.1	19.0 ± 7.9	39.8 ± 16.4	34.7 ± 15.2	0.92 ± 0.02	0.94 ± 0.02	0.96 ± 0.01	0.97 ± 0.01

[a] Abbreviations: absorption coefficient, k_{abs}; scattering coefficient, k_{sca}; and single scattering albedo, SSA (λ = 550 nm).

Therefore, vertical profiles of aerosol are required for an improved evaluation.

6. Conclusions

[44] Characterization of physicochemical properties of BC aerosol in Asian outflow was made through ground-based measurements at a remote island in Japan during March–April 2007. The concentration of aerosols and trace gases were sensitive to alternations of air mass type. BC accounted for 1–4% of the mass of PM_1 aerosol, and it reached as high as 0.5 μg m^{-3} in Asian continental (China and Korea) air masses, whereas marine air masses showed the lowest value with those at 0.16 μg m^{-3}.

[45] The size distributions of BC aerosol were quantified, revealing the mass median diameters of 200–220 nm, independent of air mass type. The shell/core diameter ratio (R) increased in Asian continental and maritime air masses, reaching ~1.6 with a core diameter (D_{BC}) of 200 nm, indicating that BC was thickly coated. Meanwhile, BC was thinly coated, with a median R of 1.3–1.4 in air masses from Japan and the free troposphere. The median values of R were higher at smaller D_{BC}. In addition, the time-dependent contributions of major coating materials were estimated, showing that organics and sulfate were the dominant coatings on BC, while sulfate was the main contributor in marine air masses.

[46] In current models, BC aerosol is treated as externally mixed or fully internally mixed with other aerosol components. However, our measurements showed the nonuniform distribution of coating thickness, depending on D_{BC} and air mass type. On the basis of theoretical calculation applying the shell/core model of Mie theory, it was suggested that coatings enhanced the absorption coefficient (k_{abs}), with an additional increase of 50–60%. The assumption of an external mixing state of BC will lead to an underestimation of the heating effects of BC. At ambient RH, water uptake by coating materials did not cause significant absorption enhancement. In addition, coatings reduced the single-scattering albedo (SSA) of PM_1 aerosol by 0.01–0.02; therefore the mixing state of BC cannot be ignored when evaluating the influence on regional climate of BC. A detailed description of the mixing state of BC is required in the models for improved estimation of direct and semi-direct effects of BC aerosol.

[47] Calculated k_{abs} values were 2–3 times higher in Asian continental air masses compared to clean air masses. The strong absorption of solar radiation by BC aerosol can lead to a heating of the atmosphere (direct effect) in the Asian outflow region. The SSA was ~0.97 in Asian continental air masses and ~0.95 in Japanese and free tropospheric air masses under ambient RH conditions. The low value of SSA would lead to reduced local low cloud amount and result in positive climate feedback (semidirect effect) in this region.

[48] **Acknowledgments.** The authors thank T. Hayasaka, N. Kikuchi, G. Nozaki, and K. Irie for their support of the field campaign. This work was supported by the Ministry of Education, Culture, Sports, Science, and Technology (MEXT), the global environment research fund of the Japanese Ministry of the Environment (B-083), and the Japanese Science and Technology Agency (JST).

References

Ackerman, A. S., O. B. Toon, D. E. Stevens, A. J. Heymsfield, V. Ramanathan, and E. J. Welton (2000), Reduction of tropical cloudiness by soot, *Science*, *288*, 1042–1047, doi:10.1126/science.288.5468.1042.

Blake, N. J., et al. (2003), NMHCs and halocarbons in Asian continental outflow during the Transport and Chemical Evolution over the Pacific (TRACE-P) field campaign: Comparison with PEM-West B, *J. Geophys. Res.*, *108*(D20), 8806, doi:10.1029/2002JD003367.

Bohren, C. F., and D. R. Hoffman (1983), *Absorption and Scattering of Light by Small Particles*, John Wiley, Hoboken, N. J.

Bond, T., and R. W. Bergstrom (2006), Light absorption by carbonaceous particles: An investigative review, *Aerosol Sci. Technol.*, *40*, 27–67, doi:10.1080/02786820500421521.

Bond, T. C., G. Habib, and R. W. Bergstrom (2006), Limitations in the enhancement of visible light absorption due to mixing state, *J. Geophys. Res.*, *111*, D20211, doi:10.1029/2006JD007315.

Clarke, A. D., et al. (2004), Size distributions and mixture of dust and black carbon aerosol in Asian outflow: Physicochemistry and optical properties, *J. Geophys. Res.*, *109*, D15S09, doi:10.1029/2003JD004378.

Cook, J., and E. J. Highwood (2004), Climate response to tropospheric absorbing aerosols in an intermediate general-circulation model, *Q. J. R. Meteorol. Soc.*, *130*, 175–191, doi:10.1256/qj.03.64.

Ehara, K., C. Hagwood, and K. J. Coakley (1996), Novel method to classify aerosol particles according to their mass-to-charge ratio: Aerosol particle mass analyzer, *J. Aerosol Sci.*, *27*(2), 217–234, doi:10.1016/0021-8502(95)00562-5.

Gao, R. S., et al. (2007), A novel method for estimating light-scattering properties of soot aerosols using a modified single-particle soot photometer, *Aerosol Sci. Technol.*, *41*, 125–135, doi:10.1080/02786820601118398.

Gysel, M., et al. (2007), Closure study between chemical composition and hygroscopic growth of aerosol particles during TORCH2, *Atmos. Chem. Phys.*, *7*, 6131–6144.

Hansen, J., M. Sato, and R. Ruedy (1997), Radiative forcing and climate response, *J. Geophys. Res.*, *102*, 6831–6864, doi:10.1029/96JD03436.

Huebert, B. J., et al. (2003), An overview of ACE-Asia: Strategies for quantifying the relationships between Asian aerosols and their climatic impacts, *J. Geophys. Res.*, *108*(D23), 8633, doi:10.1029/2003JD003550.

Jacobson, M. Z. (2000), A physically based treatment of elemental carbon optics: Implications for global direct forcing of aerosols, *Geophys. Res. Lett.*, *27*, 217–220, doi:10.1029/1999GL010968.

Janzen, J. (1979), The refractive index of carbon black, *J. Colloid Interface Sci.*, *69*(3), 436–447, doi:10.1016/0021-9797(79)90133-4.

Jayne, J. T., et al. (2000), Development of an aerosol mass spectrometer for size and composition analysis of submicron particles, *Aerosol Sci. Technol.*, *33*, 49–70, doi:10.1080/027868200410840.

Kleindienst, T. E., et al. (1999), Secondary organic aerosol formation from the oxidation of aromatic hydrocarbons in the presence of dry submicron ammonium sulfate aerosol, *Atmos. Environ.*, *33*, 3669–3681, doi:10.1016/S1352-2310(99)00121-1.

Krekov, G. M. (1993), Models of atmospheric aerosols, in *Aerosol Effects on Climate*, edited by S. G. Jennings, pp. 9–72, Univ. of Ariz. Press, Tucson.

Marley, N. A., et al. (2001), An empirical method for the determination of the complex refractive index of size-fractionated atmospheric aerosols for radiative transfer calculations, *Aerosol Sci. Technol.*, *34*, 535–549, doi:10.1080/027868201750296322.

McMurry, P. H., X. Wang, K. Park, and K. Ehara (2002), The relationship between mass and mobility for atmospheric particles: A new technique for measuring particle density, *Aerosol Sci. Technol.*, *36*, 227–238, doi:10.1080/027868202753504083.

Mikhailov, E. F., S. S. Vlasenko, I. A. Podgorny, V. Ramanathan, and C. E. Corrigan (2006), Optical properties of soot-water drop agglomerates: An experimental study, *J. Geophys. Res.*, *111*, D07209, doi:10.1029/2005JD006389.

Morino, Y., Y. Kondo, N. Takegawa, Y. Miyazaki, K. Kita, Y. Komazaki, M. Fukuda, T. Miyakawa, N. Moteki, and D. R. Worsnop (2006), Partitioning of HNO_3 and particulate nitrate over Tokyo: Effect of vertical mixing, *J. Geophys. Res.*, 111, D15215, doi:10.1029/2005JD006887.

Moteki, N., and Y. Kondo (2007), Effects of mixing state on black carbon measurement by laser-induced incandescence, *Aerosol Sci. Technol.*, *41*, 398–417, doi:10.1080/02786820701199728.

Moteki, N., and Y. Kondo (2008), Method to measure time-dependent scattering cross sections of particles evaporating in a laser beam, *J. Aerosol Sci.*, *39*, 348–364.

Moteki, N., Y. Kondo, Y. Miyazaki, N. Takegawa, Y. Komazaki, G. Kurata, T. Shirai, D. R. Blake, T. Miyakawa, and M. Koike (2007), Evolution of mixing state of black carbon particles: Aircraft measurements over the western Pacific in March 2004, *Geophys. Res. Lett.*, *34*, L11803, doi:10.1029/2006GL028943.

Nakajima, T., et al. (2007), Overview of the Atmospheric Brown Cloud East Asian Regional Experiment 2005 and a study of the aerosol direct radiative forcing in east Asia, *J. Geophys. Res.*, *112*, D24S91, doi:10.1029/2007JD009009.

Nenes, A., S. N. Pandis, and C. Pilinis (1998), ISORROPIA: A new thermodynamic equilibrium model for multiphase multicomponent inorganic aerosols, *Aquat. Geochem.*, *4*, 123–152, doi:10.1023/A:1009604003981.

Paatero, P., and U. Tapper (1993), Analysis of different modes of factor analysis as least squares fit problems, *Chemom. Intell. Lab. Syst.*, *18*, 183–194, doi:10.1016/0169-7439(93)80055-M.

Park, K., et al. (2004), Measurements of inherent material density of nanoparticle agglomerates, *J. Nanoparticle Res.*, *6*, 267–272, doi:10.1023/B:NANO.0000034657.71309.e6.

Paterson, K. G., et al. (1999), Analysis of air quality data using Positive Matrix Factorization, *Environ. Sci. Technol.*, *33*, 635–641, doi:10.1021/es980605j.

Sahu, L. K., Y. Kondo, Y. Miyazaki, M. Kuwata, M. Koike, N. Takegawa, H. Tanimoto, H. Matsueda, S. C. Yoon, and Y. J. Kim (2008), Anthropogenic aerosols observed in Asian continental outflow at Jeju Island, Korea, in spring 2005, *J. Geophys. Res.*, doi:10.1029/2008JD010306, in press.

Schnaiter, M., C. Linke, O. Möler, K.-H. Naumann, H. Saathoff, R. Wagner, U. Schurath, and B. Wehner (2005), Absorption amplification of black carbon internally mixed with secondary organic aerosol, *J. Geophys. Res.*, *110*, D19204, doi:10.1029/2005JD006046.

Schwarz, J. P., et al. (2006), Single-particle measurements of midlatitude black carbon and light-scattering aerosols from the boundary layer to the lower stratosphere, *J. Geophys. Res.*, *111*, D16207, doi:10.1029/2006JD007076.

Schwarz, J. P., et al. (2008), Coatings and their enhancement of black carbon light absorption in the tropical atmosphere, *J. Geophys. Res.*, *113*, D03203, doi:10.1029/2007JD009042.

Shiraiwa, M., Y. Kondo, N. Moteki, N. Takegawa, Y. Miyazaki, and D. R. Blake (2007), Evolution of mixing state of black carbon in polluted air from Tokyo, *Geophys. Res. Lett.*, *34*, L16803, doi:10.1029/2007GL029819.

Simpson, I. J., N. J. Blake, D. R. Blake, E. Atlas, F. Flocke, J. H. Crawford, H. E. Fuelberg, C. M. Kiley, S. Meinardi, and F. S. Rowland (2003), Photochemical production and evolution of selected C_2-C_5 alkyl nitrates in tropospheric air influenced by Asian outflow, *J. Geophys. Res.*, *108*(D20), 8808, doi:10.1029/2002JD002830.

Streets, D. G., et al. (2003), An inventory of gaseous and primary aerosol emissions in Asia in the year 2000, *J. Geophys. Res.*, *108*(D21), 8809, doi:10.1029/2002JD003093.

Takami, A., et al. (2005), Chemical composition of fine aerosol measured by AMS at Fukue Island, Japan during APEX period, *Atmos. Environ.*, *39*, 4913–4924, doi:10.1016/j.atmosenv.2005.04.038.

Takegawa, N., T. Miyakawa, Y. Kondo, J. L. Jimenez, Q. Zhang, D. R. Worsnop, and M. Fukuda (2006), Seasonal and diurnal variations of submicron organic aerosol in Tokyo observed using the Aerodyne aerosol mass spectrometer, *J. Geophys. Res.*, *111*, D11206, doi:10.1029/2005JD006515.

D. R. Blake, Department of Chemistry, University of California, Irvine, 516 Rowland Hall, Irvine, CA 92697-2025, USA.

S. Hatakeyama, Institute of Symbiotic Science and Technology, Tokyo University of Agriculture and Technology, 3-5-8 Saiwaicho, Fuchu, Tokyo 183-8509, Japan.

Y. Kondo, N. Moteki, L. K. Sahu, M. Shiraiwa, and N. Takegawa, Research Center for Advanced Science and Technology, University of Tokyo, 4-6-1 Komaba, Meguro, Tokyo 153-8904, Japan. (shiraiwa@atmos.rcast.u-tokyo.ac.jp)

A. Takami, National Institute for Environmental Studies, Onogawa 16-2, Tsukuba, Ibaraki 305-8506, Japan.

S. Yonemura, National Institute for Agro-Environmental Sciences, 3-1-3 Kannondai, Tsukuba, Ibaraki, Japan.